

The Maximal Overlap Discrete Wavelet Scattering Transform and Its Application in Classification Tasks

Leonardo Fonseca Larrubia

UNIVERSITY OF SÃO PAULO
SÃO PAULO, SP, BRAZIL

LEONARDO.LARRUBIA@USP.BR

Pedro Alberto Morettin

UNIVERSITY OF SÃO PAULO
SÃO PAULO, SP, BRAZIL

PAM@IME.USP.BR

Chang Chiann

UNIVERSITY OF SÃO PAULO
SÃO PAULO, SP, BRAZIL

CHANG@IME.USP.BR

Abstract

We present the Maximal Overlap Discrete Wavelet Scattering Transform (MODWST), whose construction is inspired by the combination of the Maximal Overlap Discrete Wavelet Transform (MODWT) and the Scattering Wavelet Transform (WST). We also discuss the use of MODWST in classification tasks, evaluating its performance in two applications: stationary signal classification and ECG signal classification. The results demonstrate that MODWST achieved good performance in both applications, positioning itself as a viable alternative to popular methods like Convolutional Neural Networks (CNNs), particularly when the training data set is limited.

Keywords: wavelets, scattering transform, discrete wavelet transform, maximal overlap discrete wavelet transform, time series, classification

1 Introduction

Most classification problems involve finding data representations that reduce variability among elements that belong to the same class while maximizing the distance among elements belonging to different classes. Highly correlated data, such as time series, images, and even volumetric data, are often more challenging due to the inherent dependence between observations and high dimensionality. Classification methods must be robust to certain deformations, as a time series shifted in time or subjected to slight deformations still belongs to the same class. Thus, time series classification techniques should aim to derive representations of the original series that are invariant to specific input deformations.

A simple way to classify time series is to use using wavelets. This can be done by defining a wavelet dictionary and using it to extract features from the time series that can later serve as input for standard classification methods. The dictionary's composition, including the type of wavelets and the classifier used in combination, is crucial for the method's success.

The Discrete Wavelet Transform (DWT) is an example of pattern extraction from a time series using compactly supported wavelets that form a basis. However, the DWT is sensitive to translations and restricted to time series of size 2^J . An alternative is the Maximal Overlap Discrete Wavelet Transform (MODWT), which is not affected by the

initial offset of the time series and can be computed for series of any size. However, this representation is highly redundant, with its coefficients being highly correlated, and it does not perform well in classification tasks. Therefore, modifications and enhancements to the MODWT are needed to improve its performance. For these enhancements, we draw inspiration from the Wavelet Scattering Transform (WST) proposed by Mallat to construct the Maximal Overlap Discrete Wavelet Scattering Transform (MODWST), which is a type of WST built using the MODWT as its base.

The plan of this work is as follows. In Section 2 we give a brief description of the Wavelet Scattering Transform and in Section 3 we describe the Discrete and the Maximal Overlap Discrete Wavelet Transforms. In Section 4 we present the Maximal Overlap Discrete Wavelet Scattering Transform. In Section 5 we give two applications and conclude in Section 6.

2 Brief Description of WST

The Wavelet Scattering Transform (WST) aims to construct representations invariant to small translations and deformations, making it an excellent tool for signal classification applications. It reduces variability among elements within the same class while effectively distinguishing those in different classes. Its construction is based on wavelet functions, i.e., functions $\psi(\cdot)$ such that $\int_{-\infty}^{\infty} \psi(t)dt = 0$ and $\int_{-\infty}^{\infty} |\psi(t)|^2 dt < \infty$.

Once an appropriate set of wavelet has been defined, WST consists of the cascade application of the modulus function and convolutions. More precisely, let $f(t)$ be a signal, ϕ an average filter, i.e. $\int_{-\infty}^{\infty} \phi(t)dt = 1$, and $\{\psi_{\lambda_k}, \lambda_k \in \Lambda_k, k = 1, \dots, n\}$ a sequence of wavelets functions, where the sequence $p = \{\lambda_1, \dots, \lambda_n\}$ is called path. The WST coefficients are obtained by

$$S_k[p]f(t) = | \dots | f \star \psi_{\lambda_1}(t) | \star \dots \star \psi_{\lambda_k}(t) | \star \phi(t),$$

where \star indicates convolution. The WST coefficients can be arranged in the vector $Sf = (S_k[p]f)_{0 \leq k \leq n}$.

Overall, the WST has a structure similar to the well-known Convolutional Neural Networks (CNN), a technique prominent in complex signal classification tasks. CNNs consist of sequences of convolutions and nonlinearities applied in cascades, obtaining a final representation that is easier to separate. In CNNs, the filter weights are learned, leading to a vast number of parameters to estimate. In contrast, the WST uses fixed wavelet filters. Mallat (2016) discusses the functioning of CNNs, drawing parallels with the WST structure, while Zarka et al. (2021) further explores this discussion.

Several studies have applied the WST in time series analysis and signal classification. Notable examples include the work of Andén and Mallat (2014), who applied the WST to audio classification problems, analyzing the GTZAN data set for music genre classification and the TIMIT data set for phoneme classification; Leonarduzzi et al. (2019), who used the WST to study entropy in financial time series; and Ahmad et al. (2017), who employed the WST to extract information from ECG data.

The two-dimensional (2D) version of the WST is also rotation-invariant, making it suitable for image analysis. In 2D WST applications, notable studies include those by Bruna and Mallat (2013), who used the WST for image classification problems, employing it as

preprocessing for analyzing the MNIST and CIFAR-10 data sets; Sifre and Mallat (2013), who described the WST’s properties and applied it to texture image classification problems; Oyallon and Mallat (2015), who analyzed the CIFAR-10 and Caltech-101 data sets for classification, exploring wavelet rotations; and the works by Oyallon et al. (2017), Oyallon et al. (2019), and Zarka et al. (2020), which created hybrid neural network architectures where the WST serves as the first CNN layer. Other studies include Villar-Corrales and Morgenshtern (2021), who used the WST for clustering images combined with “Projection onto Orthogonal Complement”; Cheng et al. (2020), who analyzed interstellar space images with the WST; and Cheng et al. (2016), who introduced an orthogonal scattering transform using Haar wavelets, a deep network computed with a hierarchy of additions, subtractions, and absolute values over pairs of coefficients, applied to the MNIST data set for classification.

There are also applications of the WST for 3D data analysis, as seen in Hirn et al. (2017), who introduced multiscale invariant dictionaries based on 3D WST for quantum estimation of chemical energies of organic molecules using training data sets; and Eickenberg et al. (2018), who presented a machine learning algorithm for predicting molecular properties inspired by density functional theory ideas, calculating the 3D WST of estimated electronic densities of molecules.

It is worth mentioning the Kymatio software (Andreux et al., 2020), which produces the WST using Morlet wavelets. It is implemented in Python and it integrates with *Numpy*, *Keras*, and *Pytorch*.

3 DWT and MODWT

Let \mathbf{X} be a time series of length $T = 2^J$. The Discrete Wavelet Transform (DWT) is an orthonormal linear transformation expressed as

$$\mathbf{W} = \mathcal{W}\mathbf{X}, \tag{1}$$

where \mathbf{W} is the vector of wavelet transform coefficients and \mathcal{W} is the orthonormal matrix, i.e., $\mathcal{W}^\top \mathcal{W} = I_T$, called the wavelet matrix.

The brute-force computation of equation (1) requires a number of operations on the order of $O(T^2)$. However, this transformation can be performed more efficiently using the well-known *pyramid algorithm*, which reduces the number of calculations to just $O(T)$. For this purpose, consider the partitioning of the vector \mathbf{W} and the matrix \mathcal{W} from (1) into, respectively, $J + 1$ subvectors and $J + 1$ submatrices, such that

$$\mathbf{W} = \begin{bmatrix} \mathbf{W}_1 \\ \mathbf{W}_2 \\ \vdots \\ \mathbf{W}_J \\ \mathbf{V}_J \end{bmatrix} = \begin{bmatrix} \mathcal{W}_1 \\ \mathcal{W}_2 \\ \vdots \\ \mathcal{W}_J \\ \mathcal{V}_J \end{bmatrix} \mathbf{X} = \mathcal{W}\mathbf{X}. \tag{2}$$

Each vector \mathbf{W}_j has a size of $T/2^j$, while each matrix \mathcal{W}_j has dimensions $T/2^j \times T$. To specify each of these components, we need to introduce the wavelet filter $\{h_l\}$, with $l = 0, \dots, L - 1$, of size L , where L is an even integer, with h_0 and h_{L-1} nonzero and $h_l = 0$ for $l < 0$ and $l \geq L$. The wavelet filter $\{h_l\}$ must satisfy the following conditions:

$$\sum_{l=0}^{L-1} h_l = 0, \quad (3)$$

$$\sum_{l=0}^{L-1} h_l^2 = 1, \quad (4)$$

$$\sum_{l=0}^{L-1} h_l h_{l+2n} = \sum_{l=-\infty}^{\infty} h_l h_{l+2n} = 0, \quad \forall n \in \mathbb{Z}. \quad (5)$$

We also need the filter $\{g_l\}$, which is closely related to the wavelet filter $\{h_l\}$ through the *quadrature mirror relationship*.

$$g_l = (-1)^{l+1} h_{L-1-l}, \quad (6)$$

while the inverse relationship is given by

$$h_l = (-1)^l g_{L-1-l}. \quad (7)$$

Letting $\mathbf{V}_0 = \mathbf{X}$, the j -th stage of pyramid algorithm, with $j = 1, \dots, J$, consists of obtaining \mathbf{W}_j and \mathbf{V}_j , of sizes $T_j = T/2^j$, such that

$$W_{j,t} = \sum_{l=0}^{L-1} h_l V_{j-1, 2t+1-l} \pmod{T_{j-1}},$$

$$V_{j,t} = \sum_{l=0}^{L-1} g_l V_{j-1, 2t+1-l} \pmod{T_{j-1}}.$$

To define the Maximal Overlap Discrete Wavelet Transform (MODWT), we first need to establish the filters $\{\tilde{h}_l\}$ and $\{\tilde{g}_l\}$ required for its construction. These filters are defined as

$$\tilde{h}_l = 2^{-j/2} h_l,$$

$$\tilde{g}_l = 2^{-j/2} g_l.$$

Once the filters $\{\tilde{h}_l\}$ and $\{\tilde{g}_l\}$ are established, we can present a definition of the MODWT, which, similar to the DWT, consists of a pyramid algorithm. Thus, letting $\tilde{\mathbf{V}}_0 = \mathbf{X}$, the level j coefficients of the MODWT are represented, respectively, by $\tilde{\mathbf{W}}_j$ and $\tilde{\mathbf{V}}_j$, whose elements are given by

$$\tilde{W}_{j,t} = \sum_{l=0}^{L-1} \tilde{h}_l \tilde{V}_{j-1, t-2^{j-1}l} \pmod{T},$$

$$\tilde{V}_{j,t} = \sum_{l=0}^{L-1} \tilde{g}_l \tilde{V}_{j-1, t-2^{j-1}l} \pmod{T}.$$

Further description and properties of DWT and MODWT can be seen in Percival and Walden (2000).

4 MODWST

Before describing the construction process of the Maximal Overlap Discrete Wavelet Scattering Transform (MODWST), we need to establish an average filter $\{\phi_l\}$, $l = 0, \dots, M$, of size $M < T$, such that

$$\sum_{l=-\infty}^{\infty} \phi_l = \sum_{l=0}^{M-1} \phi_l = 1.$$

In addition to the average filter, it is also necessary to define a stride value k , such that $1 \leq k \leq M$.

The first step is to apply the average filter $\{\phi_l\}$ to the time series \mathbf{X} of length T , obtaining the zeroth-order coefficients:

$$\tilde{S}_{(0),i} = \sum_{l=0}^{M-1} \phi_l X_{ki+l \bmod T}, \quad i = 0, \dots, \lfloor T/k \rfloor,$$

which are assembled into the vector $\tilde{\mathbf{S}}_{(0)} = [\tilde{S}_{(0);1}, \dots, \tilde{S}_{(0);\lfloor T/k \rfloor}]$.

The second step involves selecting the discrete wavelet filter $\{h_l\}$, applying the MODWT to the time series \mathbf{X} and then applying the modulus operator to each coefficient, yielding

$$|\tilde{\mathbf{W}}| = [|\tilde{\mathbf{W}}|_{(1)}, |\tilde{\mathbf{W}}|_{(2)}, \dots, |\tilde{\mathbf{W}}|_{(J)}].$$

After this, the first-order coefficients of the MODWST are obtained by the following calculation:

$$\tilde{S}_{(j_1),i} = \sum_{l=0}^{M-1} \phi_l |\tilde{\mathbf{W}}|_{(j_1);ki+l \bmod T}, \quad j_1 = 1, \dots, J, \quad i = 0, \dots, \lfloor T/k \rfloor.$$

This coefficients are assembled into the vector $\tilde{\mathbf{S}}_{(j_1)} = [\tilde{S}_{(j_1);1}, \dots, \tilde{S}_{(j_1);\lfloor T/k \rfloor}]$.

The idea of applying the modulus to the coefficients and then an average filter of size M is to measure the amount of local energy at scale i . Thus, we can interpret the coefficients $\tilde{\mathbf{S}}_{(j_1)}$ as the amount of energy at scales 2^{j_1} contained within windows of size M , which slide over the time series every k observations, i.e., each coefficient $\tilde{S}_{(j_1),i}$ represents the amount of energy at scales 2^{j_1} contained by the i -th window of size M .

The second-order coefficients are obtained by applying the same process to each vector $|\tilde{\mathbf{W}}|_{(j)}$ generated during the first-order calculation process, which can be described in the following calculation:

$$\tilde{S}_{(j_1,j_2),i} = \sum_{l=0}^{L-1} \phi_l |\tilde{\mathbf{W}}|_{(j_1,j_2);ki+l \bmod T}, \quad j_1, j_2 = 1, \dots, J, \quad i = 0, \dots, \lfloor T/k \rfloor.$$

Note that for each level $j_1 = 1, \dots, J$ of depth 1, we obtain the vectors $\tilde{\mathbf{W}}_{(j_1,j_2)}$, with $j_2 = 1, \dots, J$, which depend on the respective first-order coefficients. In other words, $\tilde{\mathbf{W}}_{(j_1,j_2)}$ form a hierarchical dependency with the level j_1 of depth 1.

We can generalize the calculation for any maximum depth m . To do so, we will use the concept of a level path, which is defined by the sequence $p_n = (j_1, \dots, j_n)$, representing a level path of maximum depth n . Therefore, given an order path $p_n = (j_1, \dots, j_n)$, an average filter $\{\phi_l\}$ of size M , a stride value $k \leq M$, a wavelet filter $\{h_l\}$ and its respective scaling filter $\{g_l\}$, both of size L , the MODWST coefficients of depth m , with $1 \leq m \leq n$, are given by

$$\tilde{S}_{p_m;i} = \sum_{l=0}^{M-1} \phi_l |\tilde{W}|_{(j_1, \dots, j_m); ki+l \pmod T}, \quad i = 0, \dots, \lfloor T/k \rfloor,$$

where $|\tilde{W}|_{(j_1, \dots, j_m);t}$ is the modulus of the coefficients $\tilde{W}_{(j_1, \dots, j_m);t}$, obtained by the following expressions:

$$\begin{aligned} \tilde{W}_{p_m;t} &= \tilde{W}_{(j_1, \dots, j_m);t} = \sum_{l=0}^{L-1} \tilde{h}_l \tilde{V}_{(j_1, \dots, j_{m-1}), t-2^{j-1}l \pmod T}, \\ \tilde{V}_{p_m;t} &= \tilde{V}_{(j_1, \dots, j_m);t} = \sum_{l=0}^{L-1} \tilde{g}_l \tilde{V}_{(j_1, \dots, j_{m-1}), t-2^{j-1}l \pmod T}, \end{aligned}$$

where

$$\tilde{V}_{(j_1, \dots, j_{m-1}, 0);t} = |\tilde{W}|_{(j_1, \dots, j_{m-1});t}, \quad 0 < j_i < J.$$

4.1 Comments

The MODWST, with a maximum depth m and stride value k , applied to a time series of size T , will contain at most $\lceil T/k \rceil (\sum_{i=1}^m \lceil \log_2 T \rceil^i + 1)$ coefficients. The zeroth depth is composed of $\lceil T/k \rceil$ coefficients, while the i -th depth is composed of $\lceil T/k \rceil \lceil \log_2 T \rceil^i$ coefficients, with $i > 0$.

The MODWT has a computational cost on the order of $O(T \log T)$. Therefore, for an MODWST with a maximum depth m , its computational cost will be on the order of $O(T(\log T)^m)$, due to its cascading calculations.

A remarkable feature is that the MODWST and WST share similar properties, due to their structures being analogous. Thus, one important property of the WST which can be extended to the MODWST is that the deeper the MODWST, the smaller the energy of the coefficients corresponding to those depths. This can be state in the following result:

$$\left| \tilde{\mathbf{S}}_{(j_1, \dots, j_m)} \right| - \left| \tilde{\mathbf{S}}_{(j_1, \dots, j_m, j_{m+1})} \right| \geq 0,$$

for all depth $m = 1, 2, \dots$ and $j_{m+1} = 1, \dots, J$. This result can also be seen as a consequence of MODWT being an energy-preserving transformation of the original series (Percival and Walden, 2000). Since MODWST does not use V_J in the cascading process, it implies that the sum of the energies of the deeper orders will always be smaller than the energy of the coefficients of the previous order.

A final feature that deserves to be highlighted is the similarity between the MODWST and a convolutional neural network (CNN). As highlighted by Mallat (2016) regarding the WST, we can observe that the wavelet filters $\{h_l\}$ resemble the convolution filters learned by CNNs, the modulus step resembles the non-linear activation functions in CNNs, and the

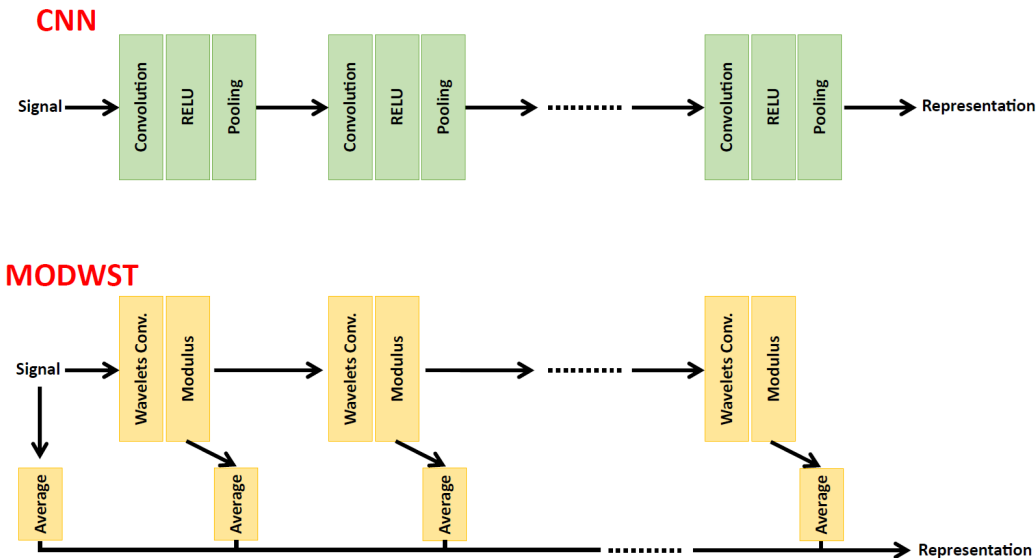


Figure 1: Comparison of the General Structures of CNNs and MODWST.

averaging filter $\{g_l\}$ corresponds to the pooling step in CNNs. Thus, the MODWST behaves analogously to CNNs but with the computational advantage of having fixed convolution weights and the disadvantage of lower flexibility. Figure 1 illustrates the comparison of the structure of MODWST and CNN.

5 Applications

We present in this section two applications aimed at evaluating the performance of MODWST in classification tasks. For these applications, we used the R software (R Core Team, 2024), with DWT and MODWT calculations performed using the `wavelism` (Whitcher, 2024) package, and classification methods were performed using the `e1071` (Meyer et al., 2024) and `kernlab` (Karatzoglou et al., 2004) packages. Additionally, we utilized the auxiliary packages `doParallel` (Corporation and Weston, 2022) and `tidyverse` (Wickham et al., 2019). The data and scripts for the applications are available at <https://github.com/laftos/MODWST>.

5.1 Stationary Processes

Andén and Mallat (2014) assert that the WST is effective for differentiating stationary processes. The goal of this application is to verify whether the MODWST can also perform well in tasks involving the discrimination of stationary signals. To evaluate this, we simulated 200 time series of size 2^{10} for each type of stationary process. The stationary processes used in this experiment were:

- **AR1a:** AR(1) process with $\phi = 0.8$ and Normal errors $(0, 0.5^2)$;
- **AR1b:** AR(1) process with $\phi = 0.4$ and Normal errors $(0, 0.5^2)$;

- **AR1c**: AR(1) process with $\phi = -0.4$ and Normal errors $(0, 0.5^2)$;
- **AR2**: AR(2) process with $\phi_1 = 0.8$, $\phi_2 = -0.9$, and Normal errors $(0, 0.5^2)$;
- **ARMA1a**: ARMA(1,1) process with $\phi_1 = 0.8$, $\theta_1 = 0.8$, and Normal errors $(0, 0.5^2)$;
- **ARMA1b**: ARMA(1,1) process with $\phi_1 = 0.8$, $\theta_1 = -0.8$, and Normal errors $(0, 0.5^2)$;
- **N1**: White noise process with Normal distribution $(0, 0.5^2)$;
- **N2**: White noise process with Normal distribution $(0, 2.5^2)$;
- **T1**: White noise process with Student's t -distribution ($\nu = 1$);
- **T3**: White noise process with Student's t -distribution ($\nu = 3$);
- **C**: White noise process with Cauchy distribution ($\gamma = 0.5$);
- **U**: White noise process with Uniform distribution $(-0.75, 0.75)$;
- **E**: White noise process with Exponential distribution ($\lambda = 2$), shifted to have zero mean;
- **B**: White noise Bernoulli process ($p = 0.5$), shifted to have zero mean;
- **P**: White noise Poisson process ($\lambda = 0.5^2$), shifted to have zero mean.

Figure 2 shows an example of the first 100 observations from each type of simulated series.

The data set was split into 80% training and 20% testing and was it was ensured an equal number of observations per class in both sets. Thus, for each class, 160 series were used for training and 40 for testing.

We used five representations of the time series:

1. **Original**: The original time series values.
2. **DWT**: The DWT coefficients, using all 2^{10} coefficients obtained.
3. **MODWT**: The MODWT coefficients, using all 11×2^{10} coefficients obtained.
4. **MODWST1**: Coefficients obtained from applying MODWST of depth 1, with a uniform averaging filter $\{\phi_l\}$ of size 2^5 and spacing $k = 2^4$, resulting in 704 coefficients.
5. **MODWST2**: Coefficients obtained from applying MODWST of depth 2, with the same averaging filter and spacing, resulting in 7104 coefficients. However, as coefficients for all observations in the path (10, 10) were computationally zero, they were excluded, leaving 7040 coefficients.

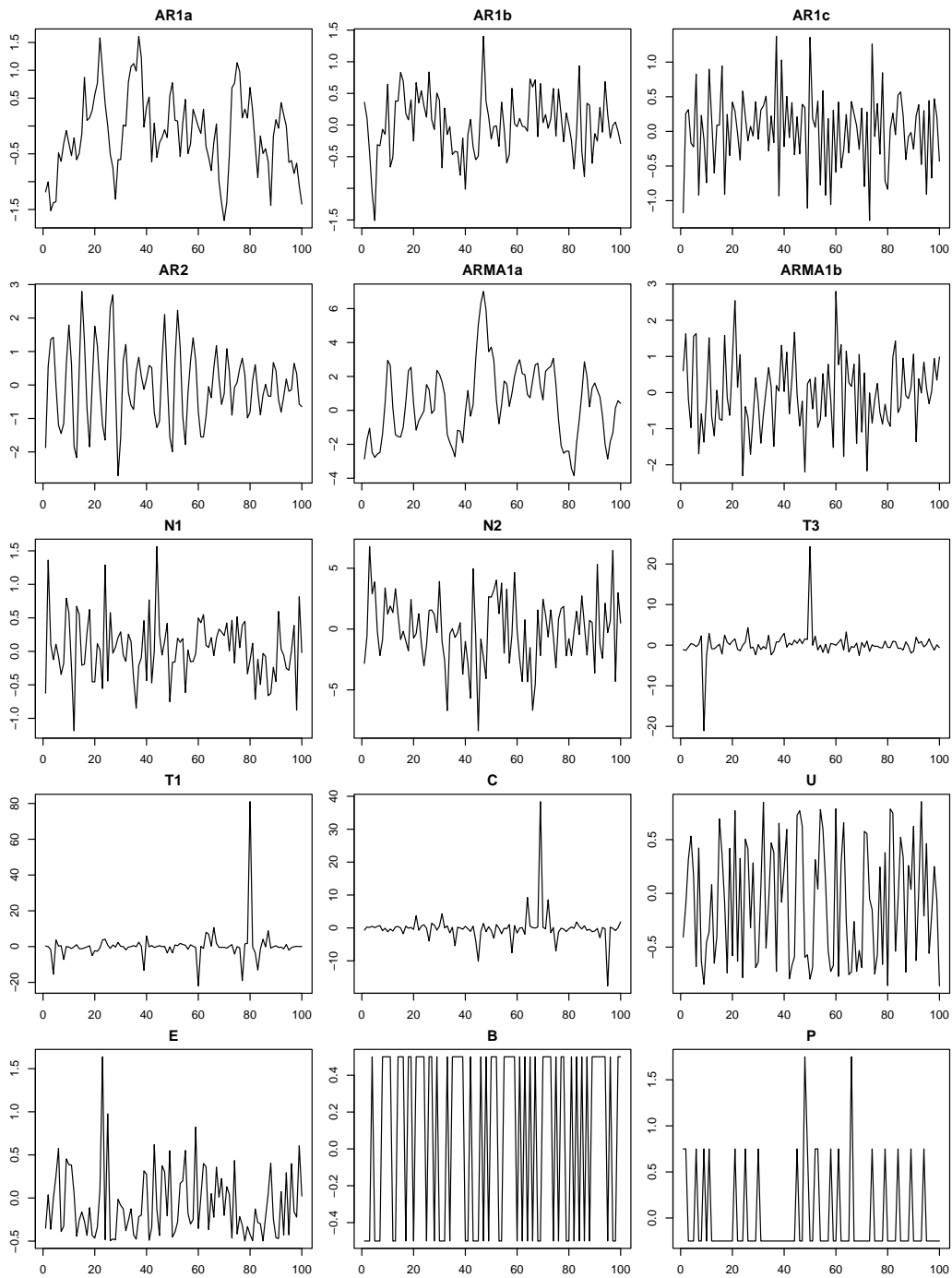


Figure 2: Example of simulated series for each stationary process.

Classifier	Accuracy (%)	LL (%)	UL (%)	Kappa
Original				
SVM-Linear	17.3	14.39	20.6	0.1143
SVM-Radial	57.8	53.77	61.8	0.5482
LDA	18.2	15.16	21.5	0.1232
Naive Bayes	63.0	59.00	66.9	0.6036
DWT				
SVM-Linear	11.5	9.06	14.3	0.0518
SVM-Radial	47.0	42.95	51.1	0.4321
LDA	11.8	9.36	14.7	0.0554
Naive Bayes	68.0	64.10	71.7	0.6571
MODWT				
SVM-Linear	11.7	9.21	14.5	0.0536
SVM-Radial	49.8	45.76	53.9	0.4625
LDA	11.8	9.36	14.7	0.0554
Naive Bayes	64.0	60.01	67.8	0.6143
MODWST1				
SVM-Linear	83.2	79.93	86.1	0.8196
SVM-Radial	70.7	66.84	74.3	0.6857
LDA	79.3	75.87	82.5	0.7786
Naive Bayes	85.0	81.89	87.8	0.8393
MODWST2				
SVM-Linear	97.3	95.71	98.5	0.9714
SVM-Radial	78.3	74.82	81.6	0.7679
LDA	92.2	89.72	94.2	0.9161
Naive Bayes	90.8	88.24	93.0	0.9018

Table 1: General results of classification performance for various methods on simulated stationary series. The lower limit (LL) and upper limit (UL) of the 95% confidence interval are reported.

	Reference														
	AR1a	AR1b	AR1c	AR2	ARMA1a	ARMA1b	B	C	E	N1	N2	P	T1	T3	U
Prediction															
AR1a	40	0	0	0	0	0	0	0	0	0	0	0	0	0	0
AR1b	0	40	0	0	0	0	0	0	0	0	0	0	0	0	0
AR1c	0	0	40	0	0	0	0	0	0	0	0	0	0	0	0
AR2	0	0	0	40	0	0	0	0	0	0	0	0	0	0	0
ARMA1a	0	0	0	0	40	0	0	0	0	0	0	0	0	0	0
ARMA1b	0	0	0	0	0	40	0	0	0	0	0	0	0	0	0
B	0	0	0	0	0	0	39	0	0	0	0	0	0	0	0
C	0	0	0	0	0	0	0	37	0	0	0	0	3	0	0
E	0	0	0	0	0	0	0	0	40	0	0	0	0	0	0
N1	0	0	0	0	0	0	0	0	0	35	0	0	0	0	4
N2	0	0	0	0	0	0	0	1	0	0	40	0	0	0	0
P	0	0	0	0	0	0	0	0	0	0	0	40	0	0	0
T1	0	0	0	0	0	0	0	2	0	0	0	0	37	0	0
T3	0	0	0	0	0	0	0	0	0	0	0	0	0	40	0
U	0	0	0	0	0	0	1	0	0	5	0	0	0	0	36

Table 2: Confusion matrix of the classification procedure using MODWST with a maximum depth of 2 in combination with the SVM classifier with a linear kernel.

The Haar wavelet was used in all wavelet-based representations. These representations were combined with four classification techniques: Support Vector Machine (SVM) with linear kernel, SVM with Gaussian kernel, Linear Discriminant Analysis (LDA) and Naive Bayes.

Table 1 summarizes the results. we can see that MODWST2 representation (up to depth 2) combined with the SVM classifier with a linear kernel achieved the highest accuracy.

Table 2 presents the classification results for the procedure that employed the MODWST with a maximum depth of 2 in combination with the SVM classifier with a linear kernel. It can be observed that the most frequent classification errors occurred only between the “Uniform” and “Normal” classes, as well as between the “Cauchy” and “t-Student(1)” classes.

5.2 ECG Time Series

We present an application of the MODWST on ECG signals using the *PTB Diagnostics* electrocardiogram database, previously processed by Kachuee et al. (2018). The goal is to classify heartbeat signals to identify potential cardiac arrhythmias.

Classifier	Accuracy (%)	LL (%)	UL (%)	Kappa
Original				
SVM-Linear	83.4	82.0	84.7	0.555
SVM-Radial	92.1	91.1	93.1	0.800
LDA	77.7	76.1	79.2	0.510
Naive Bayes	61.0	59.2	62.8	0.258
DWT				
SVM-Linear	83.4	82.0	84.7	0.555
SVM-Radial	92.1	91.1	93.1	0.800
LDA	77.7	76.1	79.2	0.510
Naive Bayes	73.8	72.2	75.4	0.458
MODWST1				
SVM-Linear	92.2	91.2	93.2	0.804
SVM-Radial	96.0	95.3	96.7	0.900
LDA	87.4	86.1	88.5	0.704
Naive Bayes	66.4	64.6	68.1	0.342
MODWST2				
SVM-Linear	98.1	97.5	98.5	0.952
SVM-Radial	97.5	96.9	98.1	0.938
LDA	96.4	95.7	97.1	0.912
Naive Bayes	64.3	62.5	66.1	0.319

Table 3: General results of classification performance for various methods applied to simulated stationary time series. The lower limit (LL) and upper limit (UL) of the 95% confidence interval are reported.

The data set consists of 14,552 time series, which 4,046 (27.8%) are from patients with normal heartbeats, and 10,506 (72.2%) are from patients with abnormal heartbeats. The original time series have varying lengths. To ensure uniformity, the latest values of the time series was padded with zeros to reach a total of 187 observations. The data set was split into 80% for training and 20% for testing.

In this study we used the same representations of the time series described in subsection 5.1, except for MODWT representation because it has a high number of coefficients and thus excessively increases the computational cost in the classification process. We also consider the same classification methods described in subsection 5.1.

The summary of the results is available in Table 3, from which we can see that the best classification method, because it presented the highest accuracy, was the MODWST2 representation, with coefficients of up to depth 2, in combination with the SVM classifier with linear kernel, having an accuracy of 98.1%. It is worth mentioning, for comparative purposes, that Kachuee et al. (2018) proposed a CNN-based classifier that had an accuracy of 95.9%.

		Reference	
		0	1
Prediction			
0	773 (26,6%)	33 (1,1%)	
1	23 (0,8%)	2082 (71,5%)	

Table 4: Confusion matrix of the classification procedure using MODWST with a maximum depth of 2 combined with the SVM classifier with a linear kernel. Classification of ECG data for the diagnosis of cardiac arrhythmia.

Table 4 shows the classification results of the procedure using MODWST with a maximum depth of 2 in combination with the SVM classifier with a linear kernel. It is observed that the types of errors were relatively balanced between the classes.

6 Conclusion

We presented the construction of the MODWST and discussed its use in classification tasks. This representation achieves strong performance in classification problems, serving as an alternative to popular methods like CNNs, especially in scenarios with limited training observations.

Further works shall focus on a deeper study of the properties of the MODWST and an evaluation of its performance in combination with other classification methods (such as neural networks and random forests) as well as in unsupervised problems, like data clustering. Additionally, there is potential to extend the MODWST to two and three dimensional cases, enabling its application to image classification and volumetric data problems.

Acknowledgments

This research was supported by CAPES (Leonardo Fonseca Larrubia) and partial support of a FAPESP grant 2023/02538-0 (Pedro Alberto Morettin and Chang Chiann).

References

- M. Z. Ahmad, A. M. Kamboh, S. Saleem, and A. A. Khan. Mallat’s scattering transform based anomaly sensing for detection of seizures in scalp eeg. *IEEE Access*, 5:16919–16929, 2017. doi: 10.1109/ACCESS.2017.2736014.
- M. Andreux, T. Angles, G. Exarchakis, R. Leonarduzzi, G. Rochette, L. Thiry, J. Zarka, S. Mallat, J. Andén, E. Belilovsky, J. Bruna, V. Lostanlen, M. Chaudhary, M. J. Hirn, E. Oyallon, S. Zhang, C. Cella, and M. Eickenberg. Kymatio: Scattering transforms in python. *Journal of Machine Learning Research*, 21(60):1–6, 2020. URL <http://jmlr.org/papers/v21/19-047.html>.

- J. Andén and S. Mallat. Deep scattering spectrum. *IEEE Transactions on Signal Processing*, 62(16):4114–4128, 2014. doi: 10.1109/TSP.2014.2326991.
- J. Bruna and S. Mallat. Invariant scattering convolution networks. *IEEE Transactions on Pattern Analysis & Machine Intelligence*, 35(08):1872–1886, aug 2013. ISSN 1939-3539. doi: 10.1109/TPAMI.2012.230.
- S. Cheng, Y.-S. Ting, B. Ménard, and J. Bruna. A new approach to observational cosmology using the scattering transform. *Monthly Notices of the Royal Astronomical Society*, 499(4):5902–5914, 10 2020. ISSN 0035-8711. doi: 10.1093/mnras/staa3165. URL <https://doi.org/10.1093/mnras/staa3165>.
- X. Cheng, X. Chen, and S. Mallat. Deep haar scattering networks. *Information and Inference: A Journal of the IMA*, 5(2):105–133, 2016. doi: 10.1093/imaiai/iaw007.
- M. Corporation and S. Weston. *doParallel: Foreach Parallel Adaptor for the 'parallel' Package*, 2022. URL <https://CRAN.R-project.org/package=doParallel>. R package version 1.0.17.
- M. Eickenberg, G. Exarchakis, M. Hirn, S. Mallat, and L. Thiry. Solid harmonic wavelet scattering for predictions of molecule properties. *The Journal of Chemical Physics*, 148(24):241732, 05 2018. ISSN 0021-9606. doi: 10.1063/1.5023798. URL <https://doi.org/10.1063/1.5023798>.
- M. Hirn, S. Mallat, and N. Poilvert. Wavelet scattering regression of quantum chemical energies. *Multiscale Modeling & Simulation*, 15(2):827–863, 2017. doi: 10.1137/16M1075454. URL <https://doi.org/10.1137/16M1075454>.
- M. Kachuee, S. Fazeli, and M. Sarrafzadeh. ECG heartbeat classification: A deep transferable representation. *CoRR*, abs/1805.00794, 2018. URL <http://arxiv.org/abs/1805.00794>.
- A. Karatzoglou, A. Smola, K. Hornik, and A. Zeileis. kernlab – an S4 package for kernel methods in R. *Journal of Statistical Software*, 11(9):1–20, 2004. doi: 10.18637/jss.v011.i09.
- R. Leonarduzzi, G. Rochette, J.-P. Bouchaud, and S. Mallat. Maximum-entropy scattering models for financial time series. In *ICASSP 2019 - 2019 IEEE International Conference on Acoustics, Speech and Signal Processing (ICASSP)*, pages 5496–5500, 2019. doi: 10.1109/ICASSP.2019.8683734.
- S. Mallat. Group invariant scattering. *Communications on Pure and Applied Mathematics*, 65(10):1331–1398. doi: <https://doi.org/10.1002/cpa.21413>. URL <https://onlinelibrary.wiley.com/doi/abs/10.1002/cpa.21413>.
- S. Mallat. Understanding deep convolutional networks. *Philosophical Transactions of the Royal Society A: Mathematical, Physical and Engineering Sciences*, 374(2065):20150203, 2016. doi: 10.1098/rsta.2015.0203. URL <https://royalsocietypublishing.org/doi/abs/10.1098/rsta.2015.0203>.

- D. Meyer, E. Dimitriadou, K. Hornik, A. Weingessel, and F. Leisch. *e1071: Misc Functions of the Department of Statistics, Probability Theory Group (Formerly: E1071), TU Wien*, 2024. URL <https://CRAN.R-project.org/package=e1071>. R package version 1.7-16.
- E. Oyallon and S. Mallat. Deep roto-translation scattering for object classification. In *2015 IEEE Conference on Computer Vision and Pattern Recognition (CVPR)*, pages 2865–2873, Los Alamitos, CA, USA, jun 2015. IEEE Computer Society. doi: 10.1109/CVPR.2015.7298904. URL <https://doi.ieeecomputersociety.org/10.1109/CVPR.2015.7298904>.
- E. Oyallon, E. Belilovsky, and S. Zagoruyko. Scaling the scattering transform: Deep hybrid networks. In *2017 IEEE International Conference on Computer Vision (ICCV)*, pages 5619–5628, Los Alamitos, CA, USA, oct 2017. IEEE Computer Society. doi: 10.1109/ICCV.2017.599. URL <https://doi.ieeecomputersociety.org/10.1109/ICCV.2017.599>.
- E. Oyallon, S. Zagoruyko, G. Huang, N. Komodakis, S. Lacoste-Julien, M. Blaschko, and E. Belilovsky. Scattering networks for hybrid representation learning. *IEEE Transactions on Pattern Analysis and Machine Intelligence*, 41(9):2208–2221, 2019. doi: 10.1109/TPAMI.2018.2855738.
- D. B. Percival and A. T. Walden. *Wavelet Methods for Time Series Analysis*. Cambridge Series in Statistical and Probabilistic Mathematics. Cambridge University Press, 2000.
- R Core Team. *R: A Language and Environment for Statistical Computing*. R Foundation for Statistical Computing, Vienna, Austria, 2024. URL <https://www.R-project.org/>.
- L. Sifre and S. Mallat. Rotation, scaling and deformation invariant scattering for texture discrimination. In *2013 IEEE Conference on Computer Vision and Pattern Recognition*, pages 1233–1240, 2013. doi: 10.1109/CVPR.2013.163.
- A. Villar-Corrales and V. I. Morgenshtern. Scattering transform based image clustering using projection onto orthogonal complement. In *Proceedings of the 2021 ACM Workshop on Intelligent Cross-Data Analysis and Retrieval, ICDAR '21*, page 24–32, New York, NY, USA, 2021. Association for Computing Machinery. ISBN 9781450385299. doi: 10.1145/3463944.3469098. URL <https://doi.org/10.1145/3463944.3469098>.
- B. Whitcher. *waveslim: Basic Wavelet Routines for One-, Two-, and Three-Dimensional Signal Processing*, 2024. URL <https://CRAN.R-project.org/package=waveslim>. R package version 1.8.5.
- H. Wickham, M. Averick, J. Bryan, W. Chang, L. D. McGowan, R. François, G. Golemund, A. Hayes, L. Henry, J. Hester, M. Kuhn, T. L. Pedersen, E. Miller, S. M. Bache, K. Müller, J. Ooms, D. Robinson, D. P. Seidel, V. Spinu, K. Takahashi, D. Vaughan, C. Wilke, K. Woo, and H. Yutani. Welcome to the tidyverse. *Journal of Open Source Software*, 4(43):1686, 2019. doi: 10.21105/joss.01686.
- J. Zarka, L. Thiry, T. Angles, and S. Mallat. Deep network classification by scattering and homotopy dictionary learning, 2020.

J. Zarka, F. Guth, and S. Mallat. Separation and concentration in deep networks, 2021.